ISAC CYTOMETRY Journal of Quantitative Cell Science PART A

MIFlowCyt

Scrippsiella acuminata versus *Scrippsiella ramonii*: A Physiological Comparison

Elena Fagín,[1*] Isabel Bravo,[1] José Luis Garrido,[2] Francisco Rodríguez,[1] Rosa I. Figueroa[1]

[1]Departamento de Microalgas Nocivas, IEO, Vigo, Spain

[2]Grupo de Fotobiología y Pigmentos del Fitoplancton, IIM-CSIC, Vigo, Spain

Received 18 October 2018; Revised 8 May 2019; Accepted 12 June 2019

Grant sponsor: Fundación Biodiversidad, Grant number: CIGUATROP; Grant sponsor: Svenska Forskningsrådet Formas, Grant number: 215-2010-824; Grant sponsor: Instituto Español de Oceanografía

Additional Supporting Information may be found in the online version of this article.

*Correspondence to: Elena Fagín, CREAF, Campus UAB, Edificio C., 08193 Bellaterra, Spain. Email: elena.fagin@gmail.com

Published online 5 July 2019 in Wiley Online Library (wileyonlinelibrary.com)

DOI: 10.1002/cyto.a.23849

Abstract

Scrippsiella is a cosmopolitan dinoflagellate genus that is able to form Harmful Algal Blooms in coastal waters. The large physiological, morphological, and genetic variability that characterizes this genus suggest the existence of cryptic species. In this study, flow cytometric analyses were carried out to compare the cell cycle and life cycle of two *Scrippsiella* strains from two different species: *Scrippsiella ramonii* (VGO1053) and *Scrippsiella acuminata* (S3V). Both species were also investigated by internally transcribed spacer rDNA sequencing and high-performance liquid chromatography-based pigment analyses. The reddish-brown color of *S. acuminata* and yellowish-green hue of *S. ramonii* were consistent with the quantitative differences determined in their pigment profiles. Our results indicate that the cell cycle is light-controlled and that it differs in the two species. S-phase was detected during the light period in both, whereas the G2/M phase occurred during the light period in *S. ramonii* but under dark conditions in *S. acuminata*. The detection of 4C stages, mobile zygotes (planozygotes), and resting cysts in *S. ramonii* (nonclonal) provided convincing evidence of sexuality in this species. Sexual related processes were not found in the clonal *S. acuminata* strain, suggesting its heterothallic behavior (i.e., the need for outcrossing). The differences in the genome size of these species were examined as well.

Key terms

Scrippsiella; cell cycle; life cycle; flow cytometry; genome size

Dinoflagellates are unicellular microalgae that belong to the larger group of eukaryotic, typically photoautotrophic microorganisms. While the morphology, physiology, biochemistry, and ecology of dinoflagellates are extremely diverse, genomic analyses have proven to be particularly challenging (1), such that only one genome has been sequenced so far, and only partially (2). The dinoflagellate nuclear genome is typically large, often >250 Gb, which is 70 times the size of the human genome (3). Other complexities and peculiarities of the dinoflagellate genome are its permanently condensed liquid-crystalline chromosomes, the lack of histones, frequent base-pair substitutions and a large number of repetitive sequences.

Dinoflagellate species use multiple adaptive strategies to survive and grow under a wide variety of environmental conditions (4,5). They notoriously form harmful algal blooms (HABs) in coastal areas around the world. HABs reflect the rapid proliferation and/or the high biomass accumulation of toxic or otherwise noxious microalgae at the sea surface or in the water column.

The high-density HABs formed by *Scrippsiella*, a genus of nontoxic, cosmopolitan marine dinoflagellates, lead to oxygen depletion and therefore fish kills (6). *Scrippsiella* blooms have been reported worldwide, including in China (7–10), Ukraine (11), Spain (12), the southern Red Sea (13), Mediterranean Sea (14,15), the Atlantic and Pacific coasts of Mexico (16–19), Australia (6), the Atlantic coast of the USA (20), and the southeast coast of Iran (21). Although little is known about the physiology of this

genus, its large physiological, morphological, and genetic variability suggest the existence of cryptic species. In fact, *Scrippsiella trochoidea*, the most common species of the genus, is a species complex that consists of a cryptic diversity and multiple species (22). Moreover, true *S. trochoidea* must be considered a heterotypic synonym of *S. acuminata* (23), this last name having priority over *S. trochoidea* (Stein 1883) as it comes from *Peridinium acuminatum*, described by Ehrenberg (1836). However, a species redefinition based on molecular phylogeny requires specific phenotypic analyses in order to correctly classify and characterize *S. acuminata.* The physiological comparison conducted in the present study revealed relevant, previously unexplored differences between two *Scrippsiella* species, *S. acuminata* and *S. ramonii*, with respect to their genome size, photosynthetic pigments, and life cycle.

As in all eukaryotic cells, dinoflagellate growth (mitotic cycle) involves DNA replication and yields two genetically identical daughter cells. Replication in eukaryotes can be divided into five stages: (1) interphase or G1, during which the vegetative cells (with a given "C" DNA content) grow and accumulate nutrients; (2) S-phase, when DNA is replicated; (3) G2, from the completion of DNA replication (2C) until the beginning of cell division; (4) mitosis, or karyokinesis, during which the nucleus divides; and (5) cytokinesis, or cytoplasmic division. However, to study dinoflagellate growth, its life cycle transitions must also be taken into account, as sexuality involves a change in the cellular DNA content. With the exception of *Noctiluca*, dinoflagellates have a haplontic life cycle, in which mitotic division occurs only in the haploid stage and the zygote is the only diploid (2 N) stage (24). Under certain environmental conditions, many species initiate a sexual cycle, during which vegetative cells differentiate into gametes that fuse to form diploid zygotes, which can either divide or form resting cysts that are deposited in the benthos (see the review by Figueroa et al. (25)). Consequently, a 2C DNA content represents either a vegetative G2 cell or a diploid (2 N, zygote), arising from the fusion of two gametes (C, N). Given that morphological differences between vegetative and sexual stages are very small or undetectable (reviewed by Bravo and Figueroa (26)), studies of the cell ploidy state are essential to identify sexual events in dinoflagellates. When, to what extent and by which route sexuality is conducted are still poorly understood. Moreover, in addition to the complex patterns of the dinoflagellate life cycle, there are numerous species-specific peculiarities. It is therefore clear that bloom formation by dinoflagellates and the ability of these organisms to adapt to a wide variety of environmental conditions cannot be fully understood without investigations of their life cycle (4,5). For example, for some species a sexual cycle has never been described, whereas for others a resting stage has never been found or it lacks a sexual origin (27). Therefore, dinoflagellate life-cycle must be studied individually in order to fully understand each species environmental response.

Among the approaches used to study the life cycle transitions of dinoflagellates are the isolation and monitoring of individual cells and determinations of the changes in the DNA content of cell populations using flow cytometry. HPLC-based pigment analyses provide chemotaxonomical fingerprint that can be associated with other phenotypic traits (e.g., changes in color and the corresponding physiological changes). Flow cytometry detects and quantifies multiple optical properties; its applications have included lipid quantification (28) and the estimation of genome size (29,30). Image flow cytometry (IFC) is a recently introduced technique that combines the fluorescence sensitivity of standard flow cytometry with the spatial resolution and quantitative morphology of digital microscopy (31). It has been used in analyses of the dinoflagellate cell cycle and in the identification of dinoflagellate life cycle stages (e.g., Ref. (32)). In the present study, we used flow cytometry, cell sorting, and IFC to examine the mitotic cycle and to determine whether a sexual cycle is a feature of *S. acuminata* and *S. ramonii.*

Methods

Experimental Organisms and Culture Conditions

The dinoflagellate species used in this study were *Scrippsiella ramonii* (strain VGO1053) and *Scrippsiella acuminata* (strain S3V). Both are regularly maintained at the culture collection of the Centro Oceanográfico de Vigo (CCVIEO; Culture Collection of Harmful Microalgae of the Spanish Institute of Oceanography). The strains were cultured at $25 \pm 1^{\circ}C$ with an irradiance of approximately 90 μmol photons m^{-2} s^{-1} and a photoperiod of 12:12 h light:dark (L:D), with the light period starting at 8:00 and ending at 20:00. The cells were grown and maintained in L1 medium (33) without added silica. The medium was prepared with NE Atlantic seawater and adjusted to a salinity of 32 psu by the addition of sterile double-distilled water.

DNA Analyses

Molecular analyses

DNA extraction, PCR amplification, and sequencing. Samples for the molecular analyses of both *Scrippsiella* strains were processed as follows. Exponentially growing cultures (1.5 ml) were harvested by centrifugation (15,871*g*, 2 min) using an Eppendorf 5424R centrifuge (Eppendorf AG, NY). The cell pellets were rinsed in 1 ml of distilled water, centrifuged again and the supernatants discarded. DNA was extracted from samples frozen overnight at $-20^{\circ}C$ according to either (1) a modified Chelex procedure, following the method of Fraga and Rodríguez (34) or (2) a CTAB protocol adapted from Doyle (35).

DNA extracts from *Scrippsiella* were quantified and checked for purity using a Nanodrop Lite spectrophotometer (ThermoScientific, Waltham, MA). The D1–D2 regions of the LSU rRNA gene were amplified using the primer pairs D1R/D2C (5′-ACCCGCTGAATTTAAGCATA-3′/5′-ACGAACGATTTGCACGTCAG-3′) (36). Internally transcribed spacer (ITS)-1/5.8S/ITS-2 rDNA regions were amplified using the primer pair ITSF01/PERK-ITS-AS (5′-GAGGAAGGAGAAGTCGTAACAAGG-3′/5′-GCTTACTTATATGCTTAAATTCAG-3′) (37). The amplification reaction mixtures (20 μl) contained 10 μl of Taq DNA polymerase master mix (2×)

(Canvax Biotech, Córdoba, Spain), 0.5 pmol of each primer, and 1–2 μl of DNA extract.

The regions of interest were amplified in an Eppendorf Mastercycler EP5345 (Eppendorf AG) as follows: 5 min of denaturation at 94°C, followed by 35 cycles of 35 s of denaturation at 94°C, a 35-s annealing step at 50°C and 1 min of elongation at 72°C, and a final elongation step of 7 min at 72°C.

The integrity of the DNA was confirmed by checking a 9-μl aliquot of each PCR sample by agarose gel electrophoresis (1.5% TAE, 80 V) and SYBR Safe DNA gel staining (Invitrogen, CA). The PCR products were purified with ExoSAP-IT (USB Corp., OH), sequenced using the Big Dye Terminator v3.1 reaction cycle sequencing kit (Applied Biosystems, Foster City, CA) and migrated in an AB 3130 sequencer (Applied Biosystems) at the CACTI sequencing facilities (Universidade de Vigo, Spain). The amplified ITS and LSU rRNA gene sequences obtained in this study were deposited in GenBank.

Phylogenetic analyses. The obtained ITS rDNA sequences were used in the phylogenetic determinations, in which sequences of *Scrippsiella ramonii* (VGO1053, 599 nt) and *S. acuminata* (S3V, 616 nt) were compared with the sequences of 30 other *Scrippsiella* spp. strains obtained from GenBank. A sequence from *Pentapharsodinium tyrrhenicum* was used as the outgroup to root the tree. ITS (ITS-1/5.8S/ITS-2 regions) sequences were aligned using BioEdit v.7.2.5 (final alignment: 567 nt). Phylogenetic model selections were performed on MEGA 7, with the TN93 + G substitution model selected for both *Scrippsiella* phylogenies (gamma shape parameter, $\gamma = 0.05$). The phylogenetic relationships were also determined using Bayesian phylogenetic inference, using the substitution models obtained by sampling across the entire general time reversible model space as described in the Mr. Bayes v3.2 manual. The Bayesian tree was produced using Mr. Bayes v3.2 (38) and the program parameters statefreqpr = dirichlet (1,1,1,1), nst = mixed, rates = gamma. One million generations were used in the analyses. Posterior probabilities were calculated from every 1,000th tree, sampled after a log-likelihood stabilization ("burn-in" phase). Maximum likelihood (ML) phylogenetic analyses were conducted in MEGA 7. Bootstrap values were estimated from 1,000 replicates. The overall topologies obtained using the ML and Bayesian inference methods were very similar. The phylogenetic tree was represented using the ML method, with bootstrap values and posterior probabilities from the Bayesian inference.

Cell cycle

Sampling. *Scrippsiella ramonii*: Cultures of *S. ramonii* that had reached 8,000–10,000 cells ml^{-1} (corresponding to the early exponential growth phase) were synchronized by placing them in complete darkness for 66 h, as described by Taroncher-Oldenburg et al. (39) and Figueroa et al. (40). Light conditions were then restored and the cells were inoculated into fresh L1 medium to a concentration of approximately 3,000 cells ml^{-1} (1.3 l in total). Sampling started 24 h after inoculation, to allow cell recovery and the initiation of cell division. An automatic water sampler (AWS, EnviroTech Instruments, Chesapeake, VA) was used to collect 24-ml samples every 2 h for 60 h, with 1 min of programmed gentle magnetic shaking just before sampling. For the determination of absolute cell numbers (cell concentration analyses), a 3-ml sample was collected manually each day of sampling, fixed with Lugol, and counted in an inverted microscope at 100× magnification using a Sedgwick-rafter chamber.

Scrippsiella acuminata: The prolonged darkness during synchronization resulted in irreversible damage to growing cells of this species. However, preliminary tests showed that this species is naturally synchronized, with few or no S-phase cells at the beginning of the light period. Therefore, *S. acuminata* cultures were not synchronized. When the cultures reached an approximate concentration of 10,000 cells ml^{-1} during a light:dark incubation (12:12), 3,000 cells were inoculated into fresh L1 medium, for a total culture volume of 1.6 l. Sampling started 24 h later, during which 25-ml samples were collected manually every 2 h for 60 h, with shaking of the cultures just before sampling. For the determination of absolute cell numbers, two 3-ml samples, the first at 11:00 and the second at 15:00, were collected manually each day, fixed in Lugol and counted as described above for *S. ramonii*.

Flow cytometry analyses and cell sorting. Samples for cell cycle and genome size studies were DNA stained and analyzed by flow cytometry. Because preliminary tests showed that *Scrippsiella* cells were highly resistant to DNA staining, the samples were first permeabilized by fixation for at least 10 min with 1% formaldehyde in a mixture with 1% "L permeabilization solution" (41). The samples were centrifuged at 9,000*g* for 10 min for the genome size analysis, and filtered through a 5.0-μm-pore-size membrane filter (Millipore, Ireland) for the cell cycle analyses. Following Kremp and Parrow (27), the retained cells were resuspended in 1 ml of a fixation solution (3:1 methanol:glacial acetic acid + 10% DMSO + 0.1% Triton-X 100) and stored for at least 12 h at 4°C to facilitate chlorophyll extraction. The cells were centrifuged at 9,000*g* for 10 min and then washed in phosphate-buffered saline (PBS) (pH 7, Sigma-Aldrich, St. Louis, MO). The pellet was resuspended in 0.33 ml of staining solution [60 μg propidium iodide ml^{-1} (Sigma-Aldrich) in PBS and 100 mg RNaseA ml^{-1} (Sigma-Aldrich) in distilled water] and maintained in darkness for at least 3 h before the analysis.

Statistical analyses, including those yielding the graphs displayed in Figure 4, were performed using the statistical and programming software R 2.1.12 (R Development Core Team, 2012) with the packages "ggplot2" and "scales," available through the CRAN repository (www.r-project.org/).

Cell sorting by flow cytometry. A SH800Z cell sorter (Sony Biotechnology Inc., Europe, United Kingdom) equipped with a 488-nm diode laser was used to analyze and sort the samples. The samples were run at medium-high pressure and data were acquired until 10,000–30,000 events in the gated

population had been recorded. Each cell cycle phase was delimited by means of a histogram of propidium iodide fluorescence. A617/30 emission filter was used for propidium iodide detection [FL3 (PI)]. According to their DNA content and nuclear fluorescence, the cells were assigned to the following peaks: 1C, S (C → 2C), 2C and 4C, in which 1C is the amount of DNA in the unreplicated gametic nucleus of an organism. ModFit LT 4.0 (Verity Software House, Topsham, ME) was used in the cell cycle analyses to calculate both the percentages of cells in the DNA fluorescence peaks and their ratios. The software FlowJo 7.6 (Tree Star, Inc.) was used in the genome size analysis to compute peak numbers, coefficients of variation (CVs), and peak ratios for the DNA fluorescence distributions in a population. Runs with CVs > 13.4 were discarded from the analyses.

Cell sorting was conducted at medium speed and in purity mode. Sorted cells with peak DNA contents of 1C, 2C, and 4C were stained with calcofluor (0.5 mg ml^{-1}) and imaged at 1,000× magnification (Leica DMR; Germany) using a microscope camera (Axiocam HRC, Zeiss Germany).

Imaging flow cytometry. A Flow Sight image flow cytometer (Amnis, Seattle, WA) was used to study the morphology of the cells in different phases of the cell cycle. The software Ideas 6.0 (Amnis) was used to process the images. The image-processing methodology followed that described in Dapena et al. (42), such that only images in focus were selected while those depicting artifacts and aggregates were discarded.

Growth parameters. The specific growth rate (43) was estimated as $K' = \frac{\ln\left(\frac{N2}{N1}\right)}{t2-t1}$, where N1 and N2 are the cells counts at times $t1$ and $t2$ of the exponential growth phase.

Divisions per day were calculated as Div $day^{-1} = K' \ln 2$.

Genome size. Duplicate exponentially growing cultures from each species were used to determine and compare the genome sizes of *S. acuminata* and *S. ramonii*. The manually collected 25-ml samples were gently mixed just before sampling at the beginning of the light period (9:00). This time point was chosen to obtain a maximum number of cells in the1C peak, used for genome size estimations, before its widening due to the onset of S-phase. The samples were stained and analyzed as described for the cell cycle analyses. Genome size was estimated by comparison with the genome sizes of two *Alexandrium minutum* strains, AMP4 and VGO577, which according to Stüken et al. (29) have an average genome size of 26.2 ± 3 and 25.7 ± 3.2 pg, respectively.

Pigment Analyses

High-performance liquid chromatography (HPLC) was used to determine pigment composition in exponentially growing cultures. The ∼40-ml samples were filtered through glass microfiber filters (0.7-μm pore-size, Filter-Lab, Spain) and stored at −20°C until use.

The pigments were extracted by the addition of 3 ml of 90% acetone to the frozen filters. After a 15-min incubation in the dark at 4°C, the filters were ground, sonicated for 5 min in an ultrasonic bath filled with a mixture of water and ice and then centrifuged (3,500*g*, 5 min). The supernatant was filtered through hydrophilic PTFE membrane filters (0.22-μm pore size) to separate the extract from the filter remnants and cell debris. The HPLC samples were prepared by mixing 130 μl of extract with 75 μl of Milli-Q water in the autosampler loop. Pigments were separated following Zapata et al. (44). The Waters Alliance HPLC system (Waters Corp.) consisted of a 2,695 separations module and a Waters 996 diode-array detector (1.2-nm optical resolution). Pigments were identified by co-chromatography with authentic standards obtained from SCORreference cultures and by diode-array spectroscopy (see Zapata et al. (44)).

Results

Phylogenetic Analysis

The phylogenetic tree obtained for *S. ramonii* strain VGO1053 and *S. acuminata* strain S3V based on their respective ITS-1/5.8S/ITS-2 rDNA regions is shown in Figure 1. It confirmed that strain VGO1053 (acc. no. MH359388) belonged to *S. ramonii*, as the ITS-1/5.8S/ITS-2 rDNA sequence was identical to that of *S. ramonii* from the Mediterranean Sea (acc. no. HQ729497). Similarly, strain S3V was confirmed as *S. acuminata*, based on the identity of its ITS-1/5.8S/ITS-2 rDNA sequence (acc. no. MH359389) to that of another *S. acuminata* sequence (acc. no. KJ189493) positioned within a subclade of *S. acuminata* (STR2, as described in Kretschmann et al. (45)).

Cell Cycle

***Scrippsiella ramonii* (strain VGO1053)**

Growth. The growth rates of the cultures were calculated during every light:dark period. From Day 1 to Day 2 of the cell cycle, the growth rate was 0.78 ± 0.05 divisions day^{-1} whereas from Day 2 to Day 3 it was higher, 0.89 ± 0.04 divisions day^{-1}.

DNA content. The nuclear fluorescence histogram (Fig. 2) revealed two main peaks in the DNA content of *S. ramonii* cells, at 1C and 2C (2C/1C = 1.9–2).

The main peak was at 1C, where the percentage of cells was between 29% and 42%. However, at the end of the light period, in the 17:00 and 19:00 samples, the 1C peak decreased and the 2C peak increased to 56%–65% of the population. The percentage of the population in the 2C peak never declined below 20%.

S-phase was detected only during the light period, with a maximum (19%) reached during the middle of this period and a minimum (5%) at the beginning of the dark period.

During the first L:D period, a 4C peak was also observed that reached a maximum of 4% at 19:00. The detection of a 4C stage indicated the existence of a sexual process in the

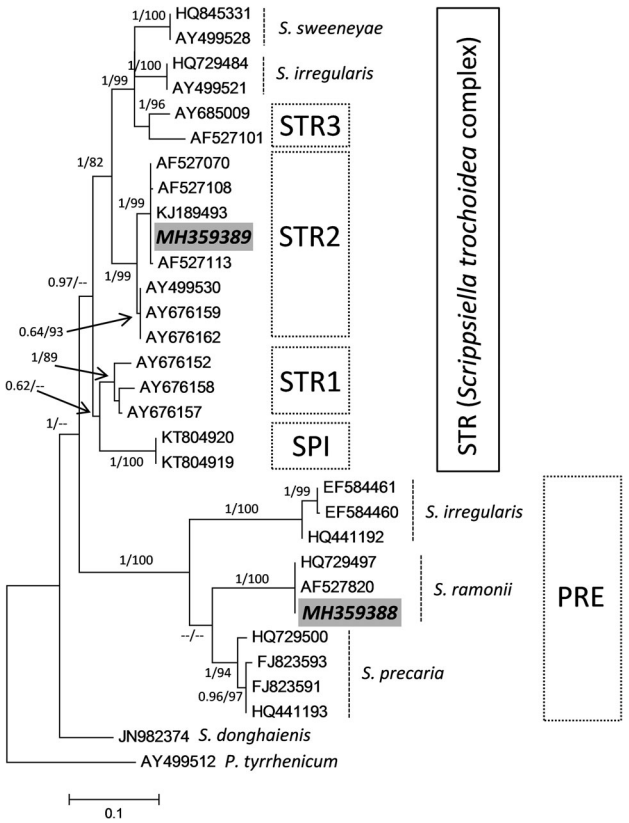

Figure 1. Phylogenetic trees inferred from ITS sequences based on maximum likelihood (ML). *Pentapharsodinium tyrrhenicum* was used as outgroup. Numbers on branches are statistical support values (Bayesian posterior probability/ML bootstrap support). Only bootstrap values >60% and posterior probabilities of 0.6 or above are shown. Hyphens indicate bootstrap/posterior probability values <60/<6. New sequences obtained in this study were highlighted in gray (*Scrippsiella acuminata* MH359389, *S. ramonii* MH359388). PRE: Clade of *Scrippsiella precaria* and its relatives; STR: Clade of *Scrippsiella acuminata* and its relatives; subclades SPI, STR1, STR2, and STR3. PRE and STR were labeled following Luo et al. (2016). Scale bar indicates number of nucleotide substitutions per site.

culture, which was also evident by the detection of resting cyst production. In addition, the IFC images (Fig. 3, image 9,867) demonstrated the existence of planozygotes, identified by their double longitudinal flagella (arrows), whereas flow cytometric cell sorting showed that the 4C cells were neither artifacts nor aggregates (Fig. 6F). The IFC images also revealed differences between the nuclear morphologies of cell populations with different DNA content peaks. Thus, 1C cells were characterized by a small, round nucleus (Fig. 3, images 79 and 87), whereas 2C cells were seen as single cells with either elongated (Fig. 3, images 1,110 and 1,309) or round (Fig. 3, images 1,317 and 9,867) nuclei or as cells in a two-celled chain (Fig. 3, images 949 and 8,633). The round nuclei of 2C cells were larger than the single nuclei of 1C cells. Resting cysts (2C content) were also identified based on their round shape and double external wall (Fig. 3, images 2,440 and 2,557).

***Scrippsiella acuminata* (strain S3V)**

Growth. The growth rate of *S. acuminata* was similar to that of *S. ramonii* albeit slower during the second L:D period. Between Days 1 and 2 of the cell cycle, the growth rate was 0.91 ± 0.06 divisions day^{-1} and between Days 2 and 3 0.71 ± 0.2 divisions day^{-1}.

DNA content. As in strain VGO1053, the prevailing peak in all strain S3V samples (except number 5, corresponding to 21:00) was at 1C, in which the percentage of C cells was between 37% and 98% (Fig. 2). The histograms from cells at the beginning of the light period (9:00, 11:00, and 13:00 samples) showed one main peak, corresponding to a 1C DNA content. However, as the cells progressed through the light period, an additional peak appeared, corresponding to a 2C DNA content (2C/1C ≥ 1.9). The maximum percentage of cells at the 2C stage was coincident with the detection of the lowest number of cells in 1C. S-phase cells were detected mostly during light conditions, from 13:00 onward.

The 2C and S-phase peaks were remarkably smaller on Day 3, which indicated that the percentage of the population remaining at the 1C stage was much higher (>68%).

A comparison of the cell cycles of *S. ramonii* and *S. acuminata* based on the percentages of cells per peak during the two light–dark periods is provided in Figure 4. In both species, the main peak during the three L:D periods was at 1C, with the percentages always >29%, while in S-phase the highest abundances occurred during the light period. By contrast, the two species differed in the timing of their 1C and 2C DNA content stages, In the case of *S. ramonii* the maximum of the 1C peak was during the dark period and for the 2C peak during light period. By contrast, for *S. acuminata*, the maximum 1C value was during the light period and the 2C maximum in the dark period. In addition, a 4C stage was not observed in *S. acuminata*.

Genome Size Comparison

Haploid DNA content was calculated by comparing the DNA content of the two strains with that of the dinoflagellate *Alexandrium minutum*, which was previously calculated by Stüken et al. (29) and thus served as a control in this study. Those authors reported that the genome of *A. minutum* strain AMP4 is slightly larger than that of *A. minutum* strain VGO577 (Fig. S1).

The haploid DNA content of *S. ramonii* and *A. minutum* was similar, 31.88 ± 0.38 pg $cell^{-1}$ (Fig. S1) whereas *S. acuminata* had a much larger genome, with a DNA content almost double (average of 59.64 ± 2.06 pg $cell^{-1}$) that of the *S. ramonii* and *A. minutum* genomes.

Nuclear Morphologies

Images of the sorted cells, captured using epifluorescence microscopy at 1,000× magnification, are shown in Figures 5 and 6. Similar to the results obtained at lower magnification with IFC, round nuclei were typical of many 1C (Figs. 5A,B and 6A–C), 2C (Fig. 6E,F), and 4C DNA (Fig. 5F) cells. However, epifluorescence allowed more detailed observations of

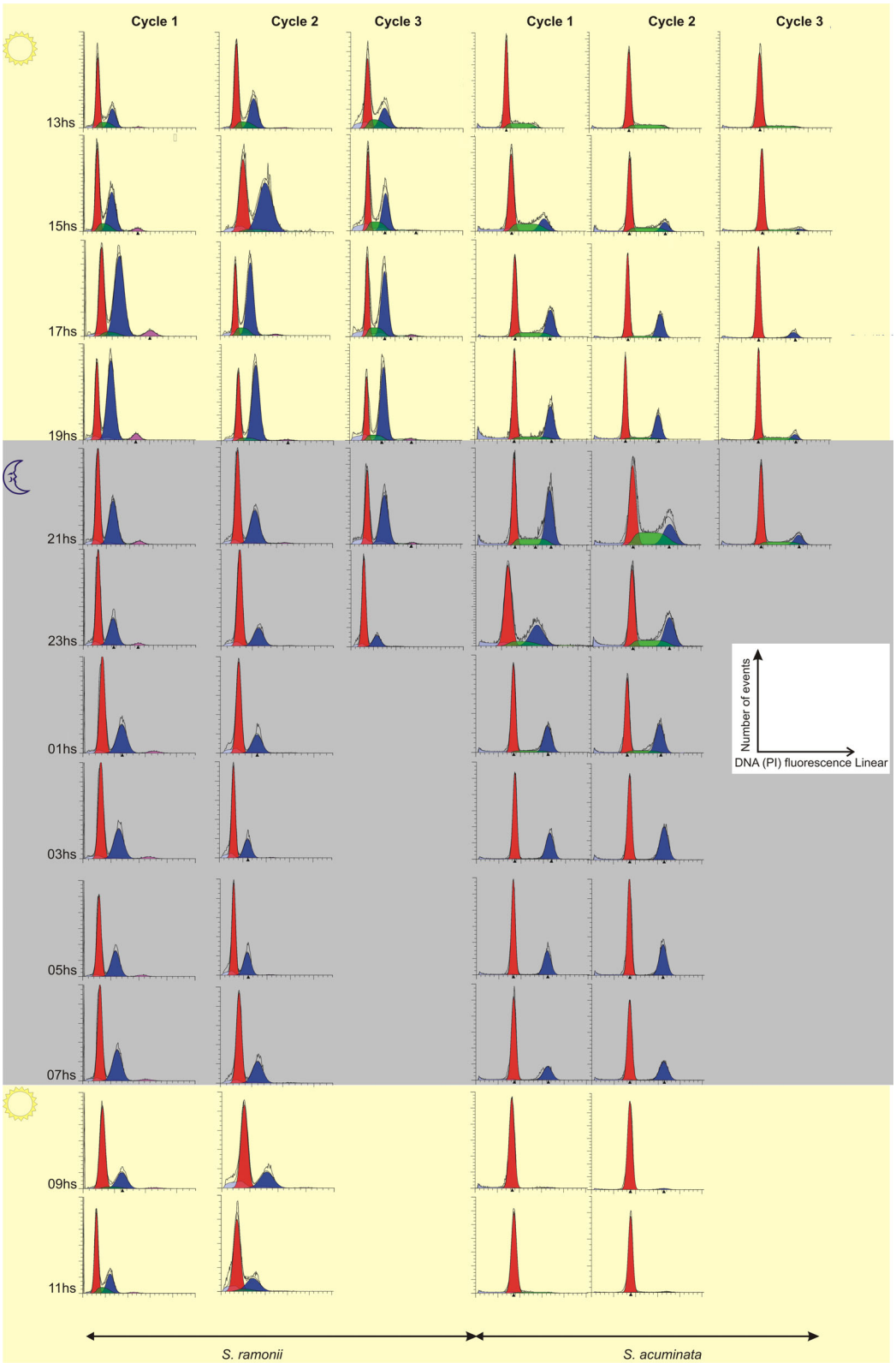

Figure 2. Cell cycle of *S. ramonii* (left) and *S. acuminata* (right). Flow histograms showing DNA intensity obtained every 2 h for the studied light:dark periods. Blue peak showed G1 (1C cells), red peak showed G2 (2C cells), and green color is the S-phase (1C → 2C) (Modfit LT 4.0 analysis). Yellow squares indicate light period and gray squares indicate dark period. Events number: 5,000–30,000. [Color figure can be viewed at wileyonlinelibrary.com]

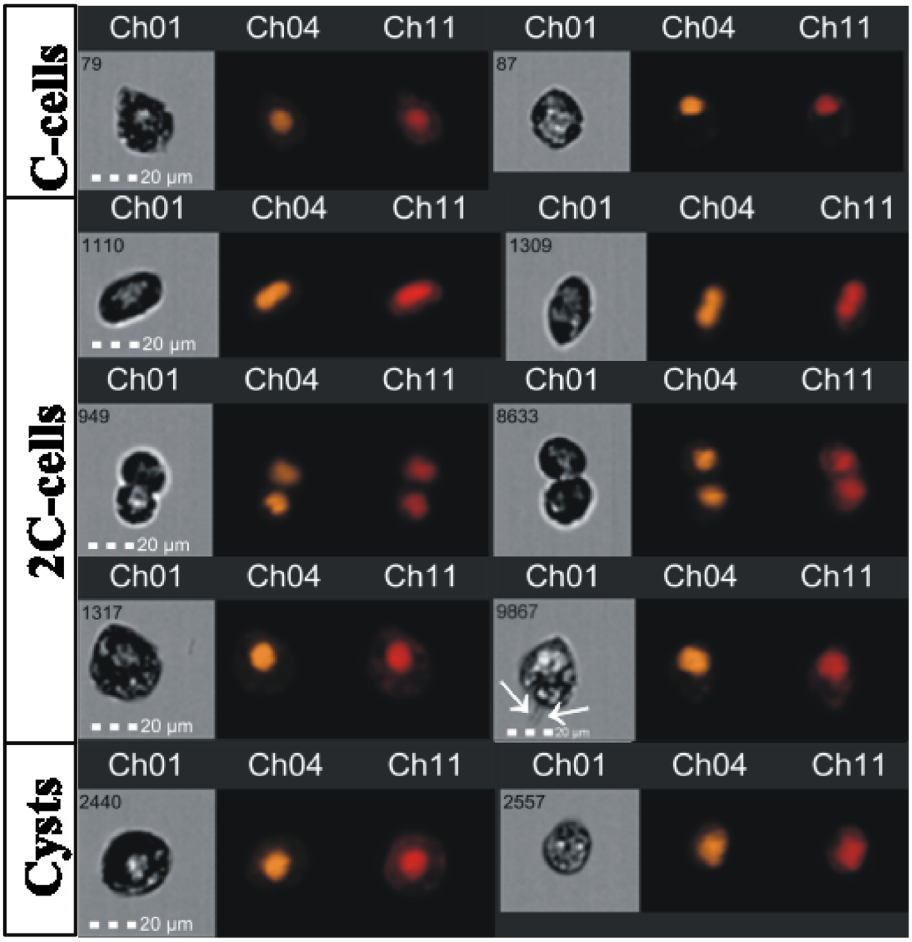

Figure 3. IFC pictures of *Scrippsiella ramonii*. IFC images of cell and nuclear morphologies using bright field (BF) microscopy and after blue (488 nm) and violet (405 nm) laser excitation. Picture 9,867 shows a planozygote with the characteristic longitudinal biflagellation. [Color figure can be viewed at wileyonlinelibrary.com]

the nuclear morphologies of *S. ramonii* 2C cells at different stages of karyokinesis (Fig. 5C,D). The main difference between the nuclei of the *S. ramonii* and *S. acuminata* was the larger nuclei of the latter at all stages of the cell cycle.

In addition to nuclear staining, the thecae of the sorted cells were stained with calcofluor to examine the relationship between nuclear morphology and thecal shape. In contrast to the differences in DNA content and nuclear size, the presence of a very thin cell wall without thecal tabulation, instead of the typical thecal pattern, was seen in the 2C dividing cells of both *S. ramonii* and *S. acuminata* (Figs. 5E and 6D). This finding suggested the occurrence of cell division after shedding of the theca and complete "de novo" formation of the theca by the daughter cells (eleuteroschisis).

Pigment Composition

Cultures of both species showed very different coloration, as *S. acuminata* (S3V) was reddish-brown while *S. ramonii* (VGO1053) had a yellowish-green hue. However, HPLC analyses showed that the same pigments occurred in the two species (Fig. S2), but that the relative proportions of the major carotenoids differed. The main accessory pigments identified in both species were peridininol, magnesium 2,4-divinylpheoporphyrin a5 monomethyl ester (MgDVP), chlorophyll c_2, peridinin, diadinoxanthin, dinoxanthin, diatoxanthin, and β,β-carotene (Fig. S2). Of these, peridinin was the main carotenoid and its molar ratio to Chl *a* was almost twice as high in *S. acuminata* as in *S. ramonii*, whereas the molar ratios of diadinoxanthin, diatoxanthin, and β,β-carotene were higher in *S. ramonii* (Table S3). The total pigment per cell was also higher in *S. acuminata*, and the peridinin content was threefold higher than that of *S. ramonii*.

Discussion

Scrippsiella Balech ex Loeblich III (Calciodinellaceae, "Peridiniales") comprises a group of thecated marine, phototrophic, dinoflagellate species producing (mostly) calcareous cysts. The taxonomy of the *Scrippsiella* genus is still unclear and the number of species has probably been underestimated (10). In our study of the different physiological parameters of *S. acuminata* and *S. ramonii*, novel information

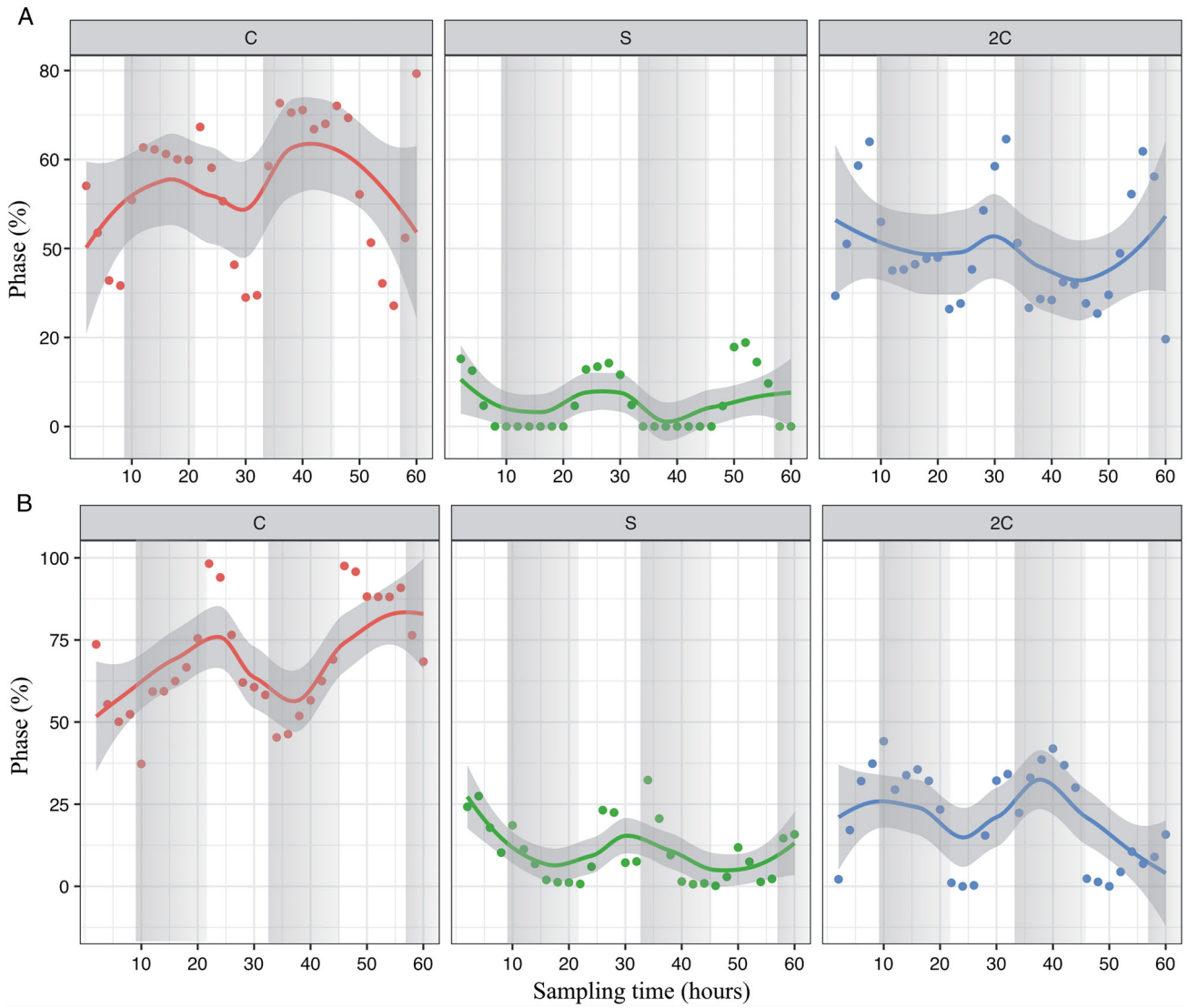

Figure 4. Comparisons between *Scrippsiella ramonii* (upper panel, **A**) and *Scrippsiella acuminata* (lower panel, **B**) cell cycles. Percentage of cells in each cell cycle stage as shown by a trend line and the standard error (gray-shaded area). The dark bars indicate the dark period. [Color figure can be viewed at wileyonlinelibrary.com]

was obtained using tools allowing the discrimination of these two *Scrippsiella* species.

Phylogenetic Analyses

The results of our phylogenetic analyses of *S. acuminata* and *S. ramonii* based on their ITS and LSU rDNA sequences are consistent with those previously reported for other *Scrippsiella* species (22,46). Thus, *S. ramonii* strain VGO1053 was shown to belong to a molecular clade ("PRE" clade (47)) that includes *S. precaria*, Montresor & Zingone, and its relatives. Strain S3V is located in the "*Scrippsiella trochoidea* complex" clade, which comprises morphologically indistinguishable (i.e., cryptic) species differentiated thus far only by genetic means (22,45,47,48). On the basis of its ITS rDNA sequences, this species was first divided into three genetic clades, STR1, STR2, and STR3 (22). However, *S. trochoidea* strains from the type locality could be ascribed only to the STR2 clade, which was then considered as that of "true" *S. trochoidea*. Later, "true" *S. trochoidea* was designated as the heterotypic synonym of *Scrippsiella acuminata* (Ehrenb.) Kretschmann, Elbr., Zinssmeister, S. Soehner, Kirsch, Kusber & Gottschling (23). For these reasons, given that in the present study strain S3V was grouped in the STR2 clade, it was identified as *Scrippsiella acuminata*, comb. nov. (Thoracosphaeraceae, Peridiniales).

Genome Size

The dinoflagellate genome can be enormous, ranging from ~1.5 pg in species of the coral symbiont *Symbiodinium* (49,50) to 225 pg in *Prorocentrum micans* (51). Our results positioned *Scrippsiella* in the middle of this distribution, with approximately 32 and 60 pg per haploid cell for *S. ramonii* and *S. acuminata*,

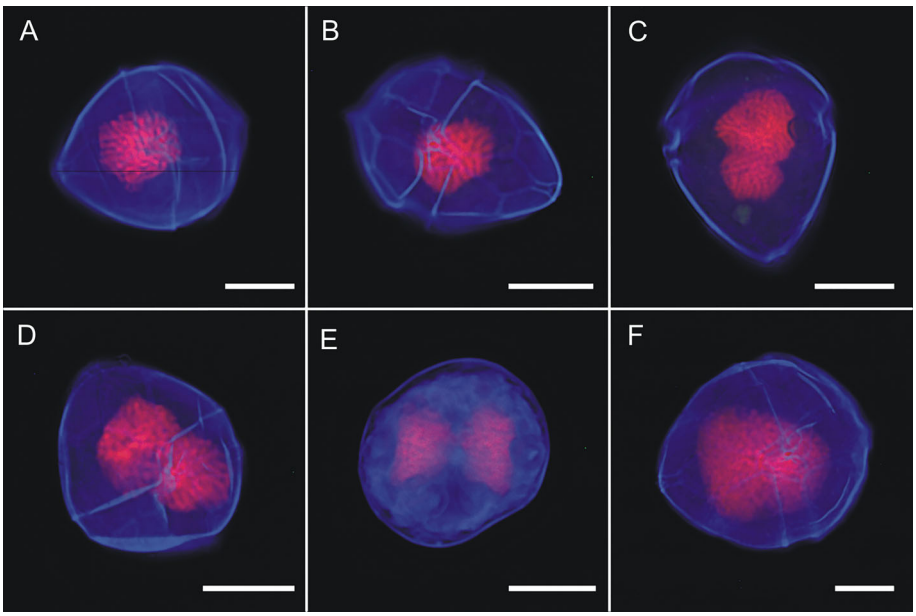

Figure 5. High power magnification images (1,000×) of *Scrippsiella ramonii* sorted cells at different cell cycle stages. **A** and **B** showed "1C" cells, **C–E** showed "2C" cells, and **F** showed a "4C" cell. DNA IP stains (red) and calcofluor (blue). Scale bars = 10 μm. [Color figure can be viewed at wileyonlinelibrary.com]

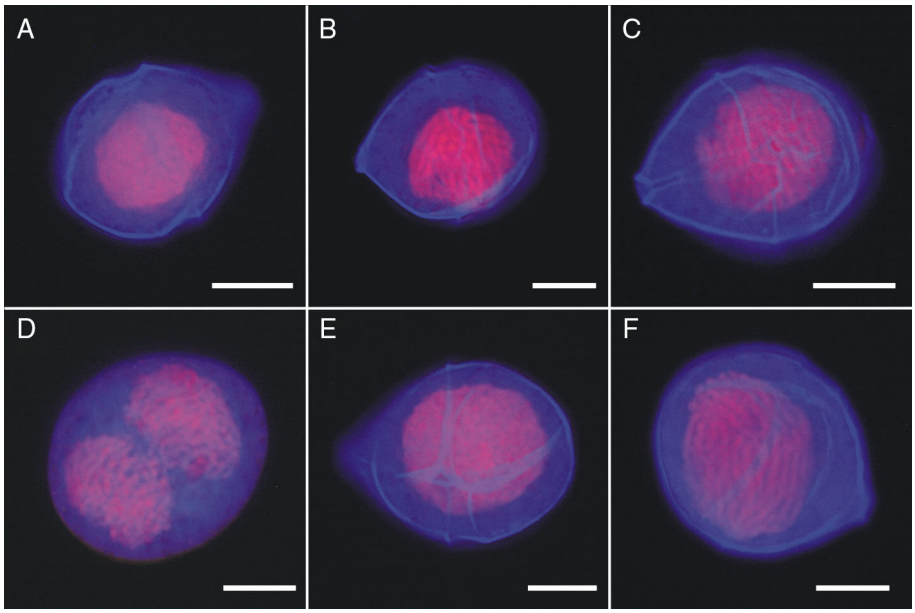

Figure 6. High power magnification (1,000×) images of *Scrippsiella acuminata* sorted cells at different cell cycle stages. **A–C** showed "1C" cells and **D–F** showed "2C" cells. DNA IP stains (red) and calcofluor (blue). Scale bars = 10 μm. [Color figure can be viewed at wileyonlinelibrary.com]

respectively. These values demonstrate the variability between dinoflagellate species of the same genus, as reported for the *Alexandrium* genus (30), and even between strains of the same species, as shown for *Alexandrium minutum* strains (29). Genome size estimates are a useful tool for comparative taxonomic studies because species identity, chromosome number, and genome size are closely associated characteristics (52). To our knowledge, this is the first report of the estimated genome sizes of *S. acuminata* and *S. ramonii.*

Cell Cycle and Life Cycle

The mitotic ratio of a given dinoflagellate population determines its division rate and, consequently, its capacity to form HABs. Another key element essential in predicting the magnitude, duration, and timing of a bloom is knowledge of the life cycle strategy of the bloom-forming species (53). Our analysis of the cell cycle and life cycle of *S. ramonii* and *S. acuminata* contributes to determinations of the similarities and differences in the growth and life cycles patterns of these species.

Cell cycle

The cell cycle of both *Scrippsiella* species showed a circadian rhythm, as reported for other phytoplankton species (54–56). Thus, the cell cycle was light-controlled over a 24-h period, with S-phase usually occurring during the light period, although at different hours depending on the species, as also shown for *Amphidinium operculatum* (57), *Karenia brevis* (58,59), *Alexandrium fundyense* (39), and *Alexandrium minutum* (32,42). In *Lingulodinium polyedra* (60) and *Protoceratium reticulatum* (61), by contrast, S-phase occurs during the dark phase. The timing of mitosis, the G2/M phase, is also variable and species-specific. This phase occurred at the end of the light period in *S. ramonii* and during the beginning of dark conditions in *S. acuminata*, as in *A. minutum* (42) and *K. brevis* (58).

During the cell cycle, mitosis returns cells in the 2C state (DNA replicated state, G2) to the 1C state (G1). While this observed in *S. acuminata* strain (S3V), it was not entirely true for *S. ramonii* (VGO1053), in which a remnant 2C phase always >20% was present in all samples of the cell cycle analysis. These 2C cells may have been either G2 cells that did not finish mitosis during a given light:dark period or sexual diploid cells. The latter option was supported by the detection of mobile zygotes (planozygotes), a life stage that either divides, but with a lower division rate than that of vegetative cells, or encysts (62,63). Alternatively, planozygotes may be able to divide mitotically, as suggested for other dinoflagellate species (32,64).

Life cycle

According to the most widespread model of the dinoflagellate life cycle, sexuality is rare and its only purpose is to create resting cysts. However, this model is now under scrutiny, as sexuality was subsequently shown to be a common phenomenon in natural blooms (65–67). Additionally, in numerous genera, including *Scrippsiella*, the division of mobile zygotes without encystment was reported (32,66,68–70). Additionally, the resting cysts of *S. hangoei* resting cysts were shown to be mostly asexual (27).

Our data confirmed the existence of sexuality in a non-clonal strain (VGO1053) of *S. ramonii*, as previously documented for this species in its original description (71). This conclusion is based on the morphological and flow cytometric characterization of a non-sexually induced and exponentially growing population, which showed the existence of biflagellated planozygotes. Additionally, the detection of 4C cells in the flow cytometric analyses evidenced zygote division (32). Sexuality in both homothallic and heterothallic strains of *S. acuminata* has been reported (48). Our results suggest that strain S3V is heterothallic, based on the apparent absence in this clonal strain of planozygotes, 4C cells, or resting cysts.

Although the *S. acuminata* strain used in this study was clonal, the *S. ramonii* strain was not, but their cell and life cycles could still be compared. Vegetative division (mitosis) is independent of the mating type and the combined use of flow cytometry and morphological analyses together with observations of resting cyst production enabled sexual studies and comparisons of the life cycles of these two strains. Moreover, sexual stages (gametes and zygotes) are also produced in some clonal-heterothallic strains of dinoflagellate species, which are thus referred to as "homozygotic," as heterothallism is defined solely by the production of resting cysts (25). Therefore, even in clonal-heterothallic cultures there could be gametes in the 1C peak and zygotes in the 2C peak. Mobile sexual life-cycle stages of dinoflagellates have hardly been studied because they cannot be identified morphologically. Therefore, we identified and estimated the presence of mobile zygotes by combining a cell cycle analysis using conventional flow cytometry with morphological parameters determined using IFC and cell sorting. Nonetheless, it was still not possible to differentiate gametes, either morphologically or based on their cell cycle attributes.

Pigments

Photosynthetic pigments can be collectively used as chemotaxonomic signatures to study dinoflagellate populations, both in the field and in culture (72). The detailed study of pigment composition explained the different coloring of both *Scrippsiella* species. It is well known that members of the *Scrippsiella* genus contain peridinin-containing plastids, which originated from secondary endosymbiosis (73,74). At the genus level, the pigment composition of different strains or species is often identical, as was the case in the present work in which the same pigments were detected in *S. acuminata* and *S. ramonii*. However, peridinin ratios normalized to Chl *a* differed between the reddish *S. acuminata* and the greenish *S. ramonii*, despite identical culture conditions. These differences are in accordance with previous studies demonstrating quantitative changes in major accessory compounds (e.g., Ref. (74)). Peridinin is a deep red carotenoid and the differences in its proportions relative to Chl *a* would account for the differences between the two species. The larger proportion of photoprotective carotenoids (diadinoxanthin and diatoxanthin) in *S. acuminata* than in *S. ramonii* indicated that irradiance acted as a stress trigger in the former (i.e., dissipation of excess excitation energy by means of the xanthophyll cycle (75)).

To conclude, in this study flow cytometric analyses were effectively applied to discriminate under laboratory conditions between cryptic dinoflagellate species belonging to the same genus. Despite the morphological similarity of *S. acuminata* and *S. ramonii*, the genome of the former was shown to be twofold larger. Additionally, the mitotic cycle was characterized by a species-specific difference in the timing of DNA replication (S-phase). Sexuality was reported in *S. ramonii* during growth, being to our knowledge the first time in which mobile zygotes of this species have been described and photographed and reported to divide. Although the *S. acuminata* strain employed in the present study was clonal, sexuality was not observed. However, it is not possible to infer that the species is strictly heterothallic, as many more strains need to be evaluated in order to be able to establish the mating type, in case, unlike in other species, it is not strain-dependent (25). Lastly, our physiological study of the two species was complemented by determinations of their pigment profiles, which

revealed additional differences between the two species and can be used to obtain additional insights into their behavior and ecological niche.

Acknowledgments

The present work was funded by the FORMAS (Sweden) project (Formas 215-2010-824), CCVIEO and CIGUATROP projects of the Instituto Español de Oceanografía and the Spanish project "Tropicalización y ciguatera en Canarias" funded by the Fundación Biodiversidad. This manuscript is a contribution of Microalgas Nocivas, IEO, Unidad Asociada al IIM (CSIC). We thank Isabel Ramilo and Pilar Rial for technical support.

Literature Cited

1. Anderson DM, Alpermann TJ, Cembella AD, Collos Y, Masseret E, Montresor M. The globally distributed genus Alexandrium: Multifaceted roles in marine ecosystems and impacts on human health. Harmful Algae 2012;14:10–35. https://doi.org/10.1016/j.hal.2011.10.012.
2. Lin S, Cheng S, Song B, Zhong X, Lin X, Li W, Li L, Zhang Y, Zhang H, Ji Z. The Symbiodinium kawagutii genome illuminates dinoflagellate gene expression and coral symbiosis. Science 2015;350(6261):691–694. https://doi.org/10.1126/science.aad0408.
3. Hackett JD, Anderson DM, Erdner DL, Bhattacharya D. Dinoflagellates: A remarkable evolutionary experiment. Am J Bot 2004;91(10):1523–1534. https://doi.org/10.3732/ajb.91.10.1523.
4. Garcés E, Bravo I, Vila M, Figueroa RI, Masó M, Sampedro N. Relationship between vegetative cells and cyst production during *Alexandrium minutum* bloom in Arenys de Mar harbour (NW Mediterranean). J Plankton Res 2004;26(6):637–645. https://doi.org/10.1093/plankt/fbh065.
5. Bravo I, Isabel Figueroa R, Garcés E, Fraga S, Massanet A. The intricacies of dinoflagellate pellicle cysts: The example of *Alexandrium minutum* cysts from a bloom-recurrent area (Bay of Baiona, NW Spain). Deep Res Part II Top Stud Oceanogr 2010;57(3–4):166–174. https://doi.org/10.1016/j.dsr2.2009.09.003.
6. Hallegraeff GM. Harmful algal blooms in the Australian region. Mar Pollut Bull 1992;25(5–8):186–190. https://doi.org/10.1016/0025-326X(92)90223-S.
7. Qi Y, Chen J, Wang Z, Xu N, Wang Y, Shen P, Lu S, Hodgkiss IJ. Some observations on harmful algal bloom (HAB) events along the coast of Guangdong, southern China in 1998. Hydrobiologia 2004;512:209–214. https://doi.org/10.1023/B:HYDR.0000020329.06666.8c.
8. Yu J, Tang D-L, Oh I-S, Yao L-J. Response of harmful algal blooms to environmental changes in Daya bay, China. Terr Atmos Ocean Sci 2007;18(5):1011–1027. https://doi.org/10.3319/TAO.2007.18.5.1011(Oc).
9. Wang ZH, Qi YZ, Yang YF. Cyst formation: An important mechanism for the termination of *Scrippsiella trochoidea* (Dinophyceae) bloom. J Plankton Res 2007;29(2):209–218. https://doi.org/10.1093/plankt/fbm008.
10. Gu H, Sun J, Kooistra WHCF, Zeng R. Phylogenetic position and morphology of thecae and cysts of Scrippsiella (Dinophyceae) species in the East China Sea. J Phycol 2008;44(2):478–494. https://doi.org/10.1111/j.1529-8817.2008.00478.x.
11. Terenko L, Terenko G. Dynamics of *Scrippsiella trochoidea* (Stein) Balech 1988 (Dinophyceae) blooms in Odessa Bay of the Black Sea (Ukraine). Oceanol Hydrobiol Stud 2009;38(S2):107–112.
12. Villarino ML, Figueiras FG, Jones KJ, Alvarezsalgado XA, Richard J, Edwards A. Evidence of in-situ Diel vertical migration of a red-tide microplankton species in Ria de Vigo (Nw Spain). Mar Biol 1995;123(3):607–617.
13. Alkawri A. Seasonal variation in composition and abundance of harmful dinoflagellates in Yemeni waters, southern Red Sea. Mar Pollut Bull 2016;112(1–2):225–234. https://doi.org/10.1016/j.marpolbul.2016.08.015.
14. Montresor M, Zingone A, Sarno D. Dinoflagellate cyst production at a coastal Mediterranean site. J Plankton Res 1998;20(12):2291–2312. https://doi.org/10.1093/plankt/20.12.2291.
15. Spatharis S, Dolapsakis NP, Economou-Amilli A, Tsirtsis G, Danielidis DB. Dynamics of potentially harmful microalgae in a confined Mediterranean Gulf-assessing the risk of bloom formation. Harmful Algae 2009;8(5):736–743. https://doi.org/10.1016/j.hal.2009.03.002.
16. Alonso-Rodríguez R, Páez-Osuna F. Nutrients, phytoplankton and harmful algal blooms in shrimp ponds: A review with special reference to the situation in the Gulf of California. Aquaculture 2003;219(1–4):317–336. https://doi.org/10.1016/S0044-8486(02)00509-4.
17. Gárate-Lizárraga I, Band-Schmidt CJ, López-Cortés DJ, Muñetón-Gómez MS. Bloom of *Scrippsiella trochoidea* (Gonyaulacaceae) in a shrimp pond in the southwestern Gulf of California, Mexico. Mar Pollut Bull 2009;58(1):145–149. https://doi.org/10.1016/j.marpolbul.2008.09.016.
18. Okolodkov YB, Merino-Virgilio F d C, Osorio-Moreno I, Herrera-Silveira JA. El género Scrippsiella (Dinoflagellata) en las aguas costeras del norte de la Península de Yucatán, sureste del Golfo de México. Bol SMF SOFILAC 2014;4:21–32.
19. Aguilar-Maldonado JA, Santamaría-del-Ángel E, González-Silvera AG, Cervantes-Rosas OD, López LM, Gutiérrez-Magness A, Sebastiá-Frasquet MT. Identification of phytoplankton blooms under the index of inherent optical properties (IOP index). Proceedings 2017;2(5):187. https://doi.org/10.3390/ecws-2-04956.
20. Marshall HG, Egerton TA. Phytoplankton blooms: Their occurrence and composition within Virginia ' s tidal tributaries Department of Biological Sciences Old Dominion University. Va J Sci 2009;60(3):149–164.
21. Attaran-Fariman G, Bolch CJS. Morphology and phylogeny of *Scrippsiella trochoidea* (Dinophyceae) a potentially harmful bloom forming species isolated from the sediments of Iran's south coast. Iran J Fish Sci 2012;11(2):252–270.
22. Gottschling M, Knop R, Plötner J, Kirsch M, Willems H, Keupp H. A molecular phylogeny of Scrippsiella sensu lato (Calciodinellaceae, Dinophyta) with interpretations on morphology and distribution. Eur J Phycol 2005;40(2):207–220. https://doi.org/10.1080/09670260500109046.
23. Kretschmann J, Elbrächter M, Zinssmeister C, Soehner S, Kirsch M, Kusber W-H, Gottschling M. Taxonomic clarification of the dinophyte *Peridinium acuminatum* Ehrenb., ≡ *Scrippsiella acuminata*, comb. nov. (Thoracosphaeraceae, Peridiniales). Phytotaxa 2015;220(3):239–256. https://doi.org/10.11646/phytotaxa.220.3.3.
24. Pfiester LA. Dinoflagellate sexuality. Int Rev Cytol 1989;114(C):249–272. https://doi.org/10.1016/S0074-7696(08)60863-3.
25. Figueroa RI, Estrada M, Garcés E. Life histories of microalgal species causing harmful blooms: Haploids, diploids and the relevance of benthic stages. Harmful Algae 2018;73:44–57. https://doi.org/10.1016/j.hal.2018.01.006.
26. Bravo I, Figueroa R. Towards an ecological understanding of Dinoflagellate cyst functions. Microorganisms 2014;2(1):11–32. https://doi.org/10.3390/microorganisms2010011.
27. Kremp A, Parrow MW. Evidence for asexual resting cysts in the life cycle of the marine peridinoid dinoflagellate, *Scrippsiella hangoei*. J Phycol 2006;42(2):400–409. https://doi.org/10.1111/j.1529-8817.2006.00205.x.
28. De La Jara A, Mendoza H, Martel A, Molina C, Nordström L, de la Rosa V, Díaz R. Flow cytometric determination of lipid content in a marine dinoflagellate. Crypthecodinium cohniiJ Appl Phycol 2003;15:433–438. https://doi.org/10.1023/A:1026007902078.
29. Stüken A, Riobó P, Franco J, Jakobsen KS, Guillou L, Figueroa RI. Paralytic shellfish toxin content is related to genomic sxtA4 copy number in *Alexandrium minutum* strains. Front Microbiol 2015;6:404. https://doi.org/10.3389/fmicb.2015.00404.
30. Figueroa RI, Cuadrado A, Stüken A, Rodríguez F, Fraga S. Ribosomal DNA organization patterns within the Dinoflagellate genus Alexandrium as revealed by FISH: Life cycle and evolutionary implications. Protist 2014;165(3):343–363. https://doi.org/10.1016/j.protis.2014.04.001.
31. Basiji DA, Ortyn WE, Liang L, Venkatachalam V, Morrissey P. Cellular image analysis and imaging by flow cytometry. Clin Lab Med 2007;27(3):653–670. https://doi.org/10.1016/j.cll.2007.05.008.
32. Figueroa RI, Dapena C, Bravo I, Cuadrado A. The hidden sexuality of *Alexandrium minutum*: An example of overlooked sex in dinoflagellates. PLoS One 2015;10(11):e0142667. https://doi.org/10.1371/journal.pone.0142667.
33. Guillard RRL, Hargraves PE. Stichochrysis immobilis is a diatom, not a chrysophyte. Phycologia 1993;32(3):234–236. https://doi.org/10.2216/i0031-8884-32-3-234.1.
34. Fraga S, Rodríguez F. Genus Gambierdiscus in the Canary Islands (NE Atlantic Ocean) with description of Gambierdiscus silvae sp. nov., a new potentially toxic epiphytic benthic Dinoflagellate. Protist 2014;165(6):839–853. https://doi.org/10.1016/j.protis.2014.09.003.
35. Doyle JJ. A rapid DNA isolation procedure for small amounts of fresh leaf tissue. Phytochem Bull 1987;19:11–15.
36. Lenaers G, Maroteaux L, Michot B, Herzog M. Dinoflagellates in evolution. A molecular phylogenetic analysis of large subunit ribosomal RNA. J Mol Evol 1989;29(1):40–51. https://doi.org/10.1007/BF02106180.
37. Kotob SI, McLaughlin SM, Van Berkum P, Faisal M. Discrimination between two Perkinsus spp. isolated from the softshell clam, *Mya arenaria*, by sequence analysis of two internal transcribed spacer regions and the 5·8S ribosomal RNA gene. Parasitology 1999;119(4):363–368.
38. Huelsenbeck JP, Ronquist F. MrBayes: Bayesian inference of phylogeny. Bioinformatics 2001;17(8):754–755. https://doi.org/10.1093/bioinformatics/17.8.754.
39. Taroncher-Oldenburg G, Kulis DM, Anderson DM. Toxin variability during the cell cycle of the dinoflagellate *Alexandrium fundyense*. Limnol Oceanogr 1997;42(5_part_2):1178–1188. https://doi.org/10.4319/lo.1997.42.5_part_2.1178.
40. Figueroa RI, Garcés E, Bravo I. Comparative study of the life cycles of *Alexandrium tamutum* and *Alexandrium minutum* (Gonyaulacales, Dinophyceae) in culture. J Phycol 2007;43(5):1039–1053. https://doi.org/10.1111/j.1529-8817.2007.00393.x.
41. Adamich M, Sweeney BM. The preparation and characterization of Gonyaulax spheroplasts. Planta 1976;130(1):1–6. https://doi.org/10.1007/BF00390837.
42. Dapena C, Bravo I, Cuadrado A, Figueroa RI. Nuclear and cell morphological changes during the cell cycle and growth of the toxic Dinoflagellate *Alexandrium minutum*. Protist 2015;166:146–160. https://doi.org/10.1016/j.protis.2015.01.001.
43. Levasseur M, Thompson PA, Harrison PJ. Physiological acclimation of marine phytoplankton to different nitrogen sources. J Phycol 1993;29(5):587–595. https://doi.org/10.1111/j.0022-3646.1993.00587.x.
44. Zapata M, Rodríguez F, Garrido JL. Separation of chlorophylls and carotenoids from marine phytoplankton: A new HPLC method using a reversed phase C8 column and pyridine-containing mobile phases. Mar Ecol Prog Ser 2000;195:29–45. https://doi.org/10.3354/meps195029.
45. Kretschmann J, Zinssmeister C, Gottschling M. Taxonomic clarification of the dinophyte *Rhabdosphaera erinaceus* K amptner, ≡ *Scrippsiella erinaceus* comb. nov (Thoracosphaeraceae, Peridiniales). Syst Biodiversity 2014;12(4):393–404. https://doi.org/10.1080/14772000.2014.934406.

46. Gottschling M, Soehner S, Zinssmeister C, John U, Plötner J, Schweikert M, Aligizaki K, Elbrächter M. Delimitation of the Thoracosphaeraceae (Dinophyceae), including the calcareous Dinoflagellates, based on large amounts of ribosomal RNA sequence data. Protist 2012;163(1):15–24. https://doi.org/10.1016/j.protis.2011.06.003.
47. Zinssmeister C, Soehner S, Facher E, Kirsch M, Meier KJS, Gottschling M. Catch me if you can: The taxonomic identity of *Scrippsiella trochoidea* (F.STEIN) A.R. LOEBL. (Thoracosphaeraceae, Dinophyceae). Syst Biodiversity 2011;9(2):145–157. https://doi.org/10.1080/14772000.2011.586071.
48. Montresor M, Sgrosso S, Procaccini G, Kooistra WHCF. Intraspecific diversity in *Scrippsiella trochoidea* (Dinopbyceae): Evidence for cryptic species. Phycologia 2003; 42(1):56–70. https://doi.org/10.2216/i0031-8884-42-1-56.1.
49. LaJeunesse TC, Lambert G, Andersen RA, Coffroth MA, Galbraith DW. Symbiodinium (Pyrrhophyta) genome sizes (DNA content) are smallest among dinoflagellates. J Phycol 2005;41(4):880–886. https://doi.org/10.1111/j.0022-3646.2005.04231.x.
50. Aranda M, Li Y, Liew YJ, Baumgarten S, Simakov O, Wilson MC, Piel J, Ashoor H, Bougouffa S, Bajic VB, et al. Genomes of coral dinoflagellate symbionts highlight evolutionary adaptations conducive to a symbiotic lifestyle. Sci Rep 2016;6:39734. https://doi.org/10.1038/srep39734.
51. Veldhuis MJW, Cucci TL, Sieracki ME. Cellular DNA content of marine phytoplankton using two new fluorochromes: Taxonomic and ecological implications. J Phycol 1997;33(3):527–541. https://doi.org/10.1111/j.0022-3646.1997.00527.x.
52. Hou Y, Lin S. Distinct gene number-genome size relationships for eukaryotes and non-eukaryotes: Gene content estimation for dinoflagellate genomes. PLoS One 2009;4(9):e6978. https://doi.org/10.1371/journal.pone.0006978.
53. Anderson DM, Chisholm SW, Watras CJ. Importance of life cycle events in the population dynamics of *Gonyaulax tamarensis*. Mar Biol 1983;76(2):179–189. https://doi.org/10.1007/BF00392734.
54. Chisholm S, Brand L. Persistence of cell-division phasing in marine-phytoplankton in continuous light after entrainment to light-dark cycles. J Exp Mar Biol Ecol 1981; 51:107–118.
55. Homma K, Hastings JW. The S phase is discrete and is controlled by the circadian clock in the marine dinoflagellate *Gonyaulax polyedra*. Exp Cell Res 1989;182(2): 635–644. https://doi.org/10.1016/0014-4827(89)90265-6.
56. Hastings J, Sweeney BM. The action spectrum for shifting the phase of the rhythm of luminescence in *Gonyaulax polyedra*. J Gen Physiol 1960;43:697–706. https://doi.org/10.1085/jgp.43.4.697.
57. Leighfield TA, Van Dolah FM. Cell cycle regulation in a dinoflagellate, *Amphidinium operculatum*: Identification of the diel entraining cue and a possible role for cyclic AMP. J Exp Mar Biol Ecol 2001;262(2):177–197. https://doi.org/10.1016/S0022-0981(01)00279-9.
58. Van Dolah FM, Leighfield TA. Diel phasing of the cell-cycle in the Florida red tide dinoflagellate. Gymnodinium breveJ Phycol 1999;35(6 Suppl):1404–1411. https://doi.org/10.1046/j.1529-8817.1999.3561404.x.
59. Van Dolah FM, Leighfield TA, Kamykowski D, Kirkpatrick GJ. Cell cycle behavior of laboratory and field populations of the Florida red tide dinoflagellate, Karenia brevis. Cont Shelf Res 2008;28(1):11–23. https://doi.org/10.1016/j.csr.2007.01.030.
60. Dagenais-Bellefeuille S, Bertomeu T, Morse D. S-phase and M-phase timing are under independent circadian control in the dinoflagellate Lingulodinium. J Biol Rhythms 2008;23(5):400–408. https://doi.org/10.1177/0748730408321749.
61. Salgado P, Figueroa RI, Ramilo I, Bravo I. The life history of the toxic marine dinoflagellate *Protoceratium reticulatum* (Gonyaulacales) in culture. Harmful Algae 2017;68:67–81. https://doi.org/10.1016/j.hal.2017.07.008.
62. Escalera L, Reguera B. Planozygote division and other observations on the sexual cycle of several species of Dinophysis (Dinophyceae, Dinophysiales). J Phycol 2008; 44(6):1425–1436. https://doi.org/10.1111/j.1529-8817.2008.00610.x.
63. Pandeirada MS, Craveiro SC, Daugbjerg N, Moestrup Ø, Calado AJ. Studies on woloszynskioid dinoflagellates VIII: Life cycle, resting cyst morphology and phylogeny of *Tovellia rinoi sp. nov.* (Dinophyceae). Phycologia 2017;56(5):533–548. https://doi.org/10.2216/17-5.1.
64. Tillmann U, Hoppenrath M. Life cycle of the Pseudocolonial Dinoflagellate Polykrikos kofoidii (Gymnodiniales, Dinoflagellata). J Phycol 2013;49(2):298–317. https://doi.org/10.1111/jpy.12037.
65. Figueroa RI, Bravo I, Ramilo I, Pazos Y, Moroño A. New life-cycle stages of *Gymnodinium catenatum* (Dinophyceae): Laboratory and field observations. Aquat Microb Ecol 2008;52(1):13–23. https://doi.org/10.3354/ame01206.
66. Figueroa RI, Garcés E, Bravo I. The use of flow cytometry for species identification and life-cycle studies in dinoflagellates. Deep Res Part II Top Stud Oceanogr 2010; 57(3–4):301–307. https://doi.org/10.1016/j.dsr2.2009.09.008.
67. Brosnahan ML, Velo-Suárez L, Ralston DK, Fox SE, Sehein TR, Shalapyonok A, Sosik HM, Olson RJ, Anderson DM. Rapid growth and concerted sexual transitions by a bloom of the harmful dinoflagellate *Alexandrium fundyense* (Dinophyceae). Limnol Oceanogr 2015;60(6):2059–2078. https://doi.org/10.1002/lno.10155.
68. Uchida T. Sexual reproduction of *Scrippsiella trochoidea* isolated from Muroran harbor, Hokkaido [Japan]. Bull Jpn Soc Sci Fish 1991;57:1215.
69. Uchida T, Matsuyama Y, Yamaguchi M, Honjo T. The life cycle of *Gyrodinium instriatum* (Dinophyceae) in culture. Phycol Res 1996;44(3):119–123. https://doi.org/10.1111/j.1440-1835.1996.tb00040.x.
70. Parrow MW, Burkholder JAM. Reproduction and sexuality in Pfiesteria shumwayae (Dinophyceae). J Phycol 2003;39(4):697–711. https://doi.org/10.1046/j.1529-8817.2003.03057.x.
71. Montresor M. Scrippsiella ramonii sp. nov. (Peridiniales, Dinophyceae), a marine dinoflagellate producing a calcareous resting cyst. Phycologia 1995;34:87–91. https://doi.org/10.2216/i0031-8884-34-1-87.1.
72. Brunet C, Johnsen G, Lavaud J, Roy S. Pigments and photoacclimation processes. In: Roy S, Llewellyn C, Egeland ES, Johnsen G, editors. Phytoplankton Pigments. Cambridge: Cambridge University Press, 2011; p. 445–471. https://doi.org/10.1017/CBO9780511732263.017.
73. Jeffrey S, Wright S, Zapata M. Microalgal classes and their signature pigments. In: Roy S, Llewellyn CA, Egeland ES, Johnsen G, editors. Phytoplankton Pigments: Characterization, Chemotaxonomy and Applications in Oceanography. Cambridge, UK: Cambridge University Press, 2011; p. 3–77. https://doi.org/10.1017/CBO9780511732263.
74. Zapata M, Fraga S, Rodríguez F, Garrido JL. Pigment-based chloroplast types in dinoflagellates. Mar Ecol Prog Ser 2012;465:33–52. https://doi.org/10.3354/meps09879.
75. Lohr M. Carotenoid metabolism in phytoplankton. In: Roy S, Llewellyn C, Egeland ES, Johnsen G, editors. Phytoplankton Pigments. Cambridge: Cambridge University Press, 2011; p. 113–162. https://doi.org/10.1017/CBO9780511732263.006.